Nanoscale Res Lett (2009) 4:526–531
DOI 10.1007/s11671-009-9275-0

NANO EXPRESS

Femtosecond Carrier Dynamics in In_2O_3 Nanocrystals

Andreas Othonos · Matthew Zervos · Demetra Tsokkou

Received: 17 December 2008 / Accepted: 9 February 2009 / Published online: 27 February 2009
© to the authors 2009

Abstract We have studied carrier dynamics in In_2O_3 nanocrystals grown on a quartz substrate using chemical vapor deposition. Transient differential absorption measurements have been employed to investigate the relaxation dynamics of photo-generated carriers in In_2O_3 nanocrystals. Intensity measurements reveal that Auger recombination plays a crucial role in the carrier dynamics for the carrier densities investigated in this study. A simple differential equation model has been utilized to simulate the photo-generated carrier dynamics in the nanocrystals and to fit the fluence-dependent differential absorption measurements. The average value of the Auger coefficient obtained from fitting to the measurements was $\gamma = 5.9 \pm 0.4 \times 10^{-31}$ cm^6 s^{-1}. Similarly the average relaxation rate of the carriers was determined to be approximately $\tau = 110 \pm 10$ ps. Time-resolved measurements also revealed $\sim$25 ps delay for the carriers to reach deep traps states which have a subsequent relaxation time of approximately 300 ps.

Keywords In_2O_3 nanocrystals · Carrier dynamics · Femtosecond differential absorption spectroscopy · Auger coefficient

A. Othonos (✉) · D. Tsokkou
Department of Physics, Research Centre of Ultrafast Science, University of Cyprus, P.O. Box 20537, Nicosia 1678, Cyprus
e-mail: othonos@ucy.ac.cy

M. Zervos
Department of Mechanical and Manufacturing Engineering, Materials Science Group, Nanostructured Materials and Devices Laboratory, University of Cyprus, P.O. Box 20537, Nicosia 1678, Cyprus

Introduction

Indium oxide In_2O_3 is considered an important n-type wide-band gap semiconductor which has received a great deal of attention over the past few years due to its technological application in optoelectronic devices [1, 2] and sensors [3]. Indium oxide is useful in these devices because of its high transparency in the visible part of the spectrum, high electric conductance, and its strong interaction with certain gas molecules. Furthermore, the growth of In_2O_3 nanocrystals (NCs) and nanowires (NWs) for sensor applications has also received attention in view of the large surface-area-to-volume ratio. These nanostructures have shown great promise for chemical and biological sensors [4–8] and as a result have attracted great interest by the nanostructure and sensing communities [9–18]. For example, In_2O_3 NWs configured as gas sensors have demonstrated greater room temperature sensitivity and selectivity than their commercial tin oxide thin-film counterparts. In addition, they have shown to be effective ultraviolet photo detectors [19].

Despite the extensive use of In_2O_3 as a transparent conducting material in optoelectronic devices, such as light emitting diodes, photovoltaic cells, liquid crystal displays, there has not been any detailed study on the photoinduced carrier dynamics. Therefore in this study we investigate the ultrafast carrier dynamics in In_2O_3 nanocrystals (average diameter $\sim$500 nm) using two color pump-probe absorption spectroscopy [20–22], where the various important relaxation mechanisms have been identified. We find that Auger recombination appears to play a crucial role in the recovery of the photo-generated carriers in the In_2O_3 NCs within the first tens of ps and the Auger coefficient is $5.9 \pm 0.4 \times 10^{-31}$ cm^6 s^{-1}.

Experimental Procedure

The In_2O_3 NCs were grown using an atmospheric pressure chemical vapor deposition (APCVD) reactor which consists of four mass flow controllers (MFC's) and a horizontal quartz tube furnace, capable of reaching a maximum temperature of 1100 °C. Initially fine In powder (Aldrich, Mesh—100, 99.99%) was weighed and loaded into a quartz boat together with a square piece of quartz which was positioned about 10 mm from the In. Then the boat was loaded into the quartz tube reactor and positioned directly above the thermocouple used to measure the heater temperature at the center of tube. After loading the boat at room temperature (RT), Ar (99.999%) was introduced at a flow rate of 500 standard cubic centimeters per minute (sccm) for 10 min in order to purge the tube. Following this the temperature was ramped to 1000 °C in a reduced Ar flow of 100 sccm. Upon reaching T_G, the flow of Ar was reduced to 90 sccm and O_2 introduced at a flow of 10 sccm for another 60 min after which the O_2 flow was cut off and the quartz tube was allowed to cool down over at least 60 min in an inert gas flow of Ar, 100 sccm. The sample was removed only when the temperature was lower than 100 °C. A typical scanning electron microscope (SEM) image of the In_2O_3 NCs is shown in Fig. 1.

The average diameter of the NCs grown on the quartz substrate is approximately 500 nm whereas their estimated density is 8×10^7 NC/cm^2. Further details on the growth and structure are given elsewhere [23]. Steady-state transmission measurements provided an estimate of the NCs band gap from a plot of the square of the absorption versus photon energy to be approximately 3.5 eV [24]. Furthermore the absorption curve shown as an inset in Fig. 1 depicts non-zero absorption below the band gap. Room temperature photoluminescence revealed a broad band luminescence covering a range between 350 and 460 nm with a peak at 390 nm. This is attributed to oxygen defects contained in the NCs, in agreement with previous reports [25–28] which suggest that oxygen vacancies are formed due to the incomplete oxidation during growth which act as donors resulting in the additional states below the band gap. In addition indium vacancies or interstitials in the NCs, may also be a contributing factor to the presence of the energy states below the band gap [29]. Thus the conduction band tail extends over a large wavelength range resulting in PL due to the recombination from these defect states.

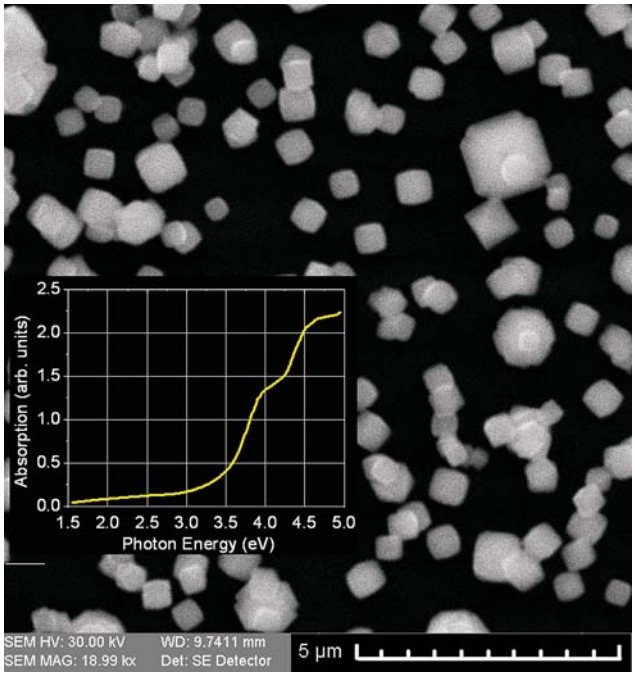

Fig. 1 SEM images of In_2O_3 NCs grown by direct oxidation of In with O_2 at 1000 °C with an average diameter of 500 nm. The inset at the lower corner corresponds to the absorption of the NCs obtained from steady-state transmission measurements

At this point we should mention that the In_2O_3 NCs, given their relatively large size with the respect to the exciton Bohr radius ($\sim$2.4 nm), are not quantum confined; therefore the data from these structures can be analyzed within the framework of bulk-like material.

In this study, the dynamic behavior of carriers in In_3O_2 nanocrystals following femtosecond pulse excitation is investigated through the temporal behavior of induced absorption [20–22]. The experiments were carried using an ultrafast amplifier system running at 5 kHz. The source of short pulses was a self-mode-locked Ti:Sapphire oscillator generating 45 fs pulses at 800 nm. Part of the amplified energy was used in an *Optical Parametric Amplifier* system providing wavelength tunability in the UV range of the spectrum and thus a means of exciting the In_3O_2 nanocrystals. The rest of the energy was used to generate 400 nm from a BBO crystal and white light super continuum. The UV pulses from the OPA were used as the pump energy to excite the nanocrystals given that the expected band gap of this material is around 3.5 eV. The VIS–IR white light super continuum (500–1000 nm) which was use to probe the excited region was generated by focusing the 800 nm pulses on a 1-mm sapphire plate. Similarly a super continuum in the UV region of the spectrum was also generated with 400 nm pulses. The white light probe beam is used in a non-collinear geometry, pump-probe configuration, where the pump beam was generated from the OPA. Optical elements such as focusing mirrors were utilized to minimize dispersion effects and thus minimize the broadening of the laser pulse. The reflected and transmission beams were separately directed onto their respective detectors after passing through a band pass filter selecting the probe wavelength from the white light. The differential

reflected and transmission signals were measured using lock-in amplifiers with reference to the optical chopper frequency of the pump beam. The temporal variation in the photo-induced absorption is extracted using the transient reflection and transmission measurements, which is a direct measure of the photoexcited carrier dynamics within the probing region [20–22]. Precision measurements of the spot size on the sample of the pump beam along with measurements of reflection and transmission at the pump wavelength provided accurate estimation of the absorbed fluence for the experiments in this study.

Results and Discussion

Figure 2 shows typical time-resolved differential absorption measurements of the In_2O_3 nanocrystals for different photon probing energies. The excitation was accomplished with 3.81 eV (325 nm) photons under a pump fluence of 0.250 mJ/cm^2. Clearly from the data in Fig. 2, we notice two distinct regions of different behavior.

The first region corresponds to probing wavelengths below ~400 nm where the induced absorption change appears to be negative, and the second region corresponds to longer probing wavelengths where the change appears to be positive. For both probing regions there is an initial sharp change which is pulse-width limited reaching a maximum value, and then followed by a slow recovery toward equilibrium which persists over tens of picoseconds. The negative change in the induced absorption corresponds to what we refer to as "*state filling*". This is

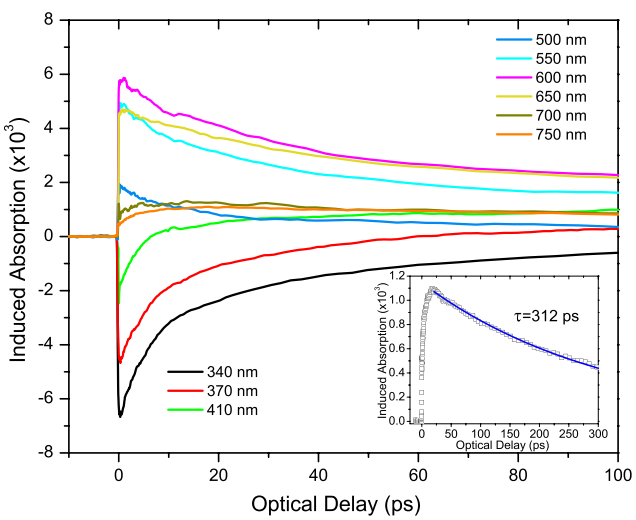

Fig. 2 Differential absorption signal vs. time delay for different photon wavelengths in In_2O_3 nanocrystals. Photoexcitation was accomplished with 3.81 eV (325 nm) photons under a pump fluence of 250 μJ/cm^2 at room temperature. The inset shows a fit to the differential absorption data for probing wavelength at 750 nm by a single-exponential decay

associated with the occupation of states of the In_2O_3 NCs by the photogenerated carriers following photoexcitation by the ultrafast laser pulse whose energy is above the band gap. Once the carriers occupy states that were normally unoccupied the absorption at the probing wavelength will appear reduced. Therefore, monitoring this negative change in absorption as a function of delay between the excitation and probing pulse is a direct measure of the temporal evolution of the photo-generated carriers at the probing wavelength state. On the other hand, if the probing energy is smaller than the band-gap energy, direct coupling from the valence band states to conduction band states will not be possible, therefore state filling will not be observed. However, under such probing conditions a positive change in the induced absorption maybe observable. This is due to secondary excitation of the photo-generated carriers to higher energy states due to the probing pulse. This positive photo-induced change depends on the number of photo-generated carriers present in the initial state and the coupling efficiency between the initial and final state. Therefore, the recovery signal is again a direct measure of the decay of the photo-generated carriers from the probing energy state. Here we should point out that in some cases state filling may be possible below the band gap when there are available energy states below the band edge which is the case for the In_2O_3 NCs. The transient differential absorption measurements (Fig. 2) show state filling for probing wavelengths as long as 410 nm.

The recovery of state filling signal as seen for the shorter probing wavelengths (340 nm, 370 nm) in Fig. 2 consists of two distinct temporal components, a fast and a much slower component. The fast component as we will show later on in this study is mainly due to Auger recombination, whereas the slower component which is of the order of 100 ps is associated with recombination or capture of the photo-generated carriers by various traps or surface-related states. It appears with increasing probing wavelength, the coupling from the valence bands to the available energy states below the band gap becomes weaker thus the state filling is reduced (this is in agreement with the broad photoluminescence spectra which drops to zero at ~460 nm). At the same time the contribution of secondary excitations increases, possibly, due to available higher energy states in the bands that the photo-generated carriers may couple by conserving energy and momentum. This is clearly evident from the observed increase in positive-induced absorption with increasing probing wavelength (Fig. 2). We should also point out that at some point both effects may be present as seen in Fig. 2 at the probing wavelength of 410 nm. Furthermore, there appears to be a peak of positive-induced absorption at 600 nm which is attributed to a larger density of the coupled states at the particular probing wavelength.

The recovery seen in the positive photo-induced absorption, for the longer probing wavelengths, contains both temporal components seen for the shortest probing wavelengths; however, the fast Auger recombination component is much less pronounced. This is mainly because the number of carriers distributed among the probing states which are located below the band gap is less than that in the case of state filling which occurs near the band edge where most of the carriers relax before captured by traps or recombine. In addition near the band edge the probe couples to the electron and hole states, while at longer wavelengths it only interacts with electrons or holes separately. Since Auger recombination has a cubic carrier density dependence, this will cause a pronounced change on the temporal evolution of the photo-induced absorption.

It is also interesting to point out that the recovery of the induced absorption is much longer ($\sim$312 ps, see inset in Fig. 2) at the probing wavelength of 700 and 750 nm. Furthermore, the maximum signal appears to occur around 25 ps after the excitation pulse. The photo-generated carriers required a relatively long time to reach the probing states. This suggests that we are probing states that are much different than those we are probing with the shorter wavelengths where the maximum signal appears to be instantaneous (pulse-width limited). It is believed that we are probing deep traps states where the initial photo-generated carriers in the NCs have relaxed, at which point subsequent relaxation from these states is on the order of 300 ps.

Furthermore, we have investigated time-resolved dynamics at various excitation wavelengths with similar results. However, with increasing wavelength the signal becomes weaker. No measureable differential absorption signal was detected for pump wavelengths longer than 360 nm.

To further investigate the dynamics of the photo-generated carriers we have performed intensity measurements at various probing wavelengths. Typical measurements with excitation at 325 nm and probing at 350 nm are shown in Fig. 3. In the inset of Fig. 3 we display the normalized results, which clearly indicate the effect of Auger recombination in these NCs. To analyze these data and obtain a value for the Auger coefficient we have utilized a model which consists of a simple differential equation incorporating the photo-generated carrier behavior following excitation by an ultrashort laser pulse:

$$\frac{\mathrm{d}N(t,z)}{\mathrm{d}t} = g(t,z) + D\frac{d^2N}{dz^2} + -\frac{N}{\tau} - \gamma N^3$$

where *N(t,z)* corresponds to the carrier density which is a function of time and position from the surface of the sample. The carrier generation term is represented by the spatial and temporal function *g(t,z)*, associated with the optical pulse

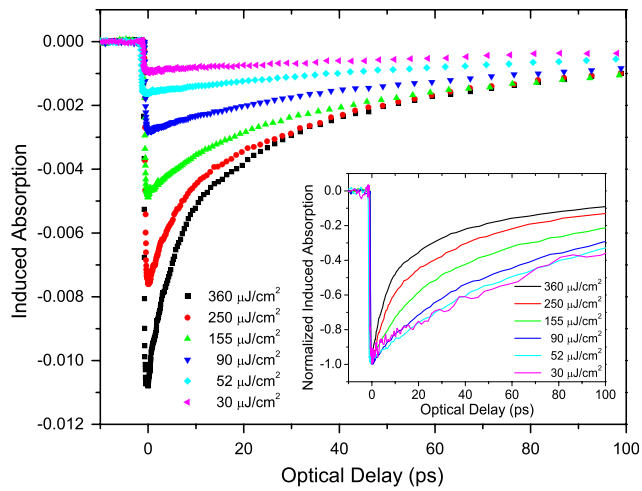

Fig. 3 Time-resolved differential absorption of In_2O_3 nanocrystals excited with 325 nm and probe at 350 nm at different fluences. The inset shows the same measurements normalized which clearly indicate the effect Auger recombination with increasing fluences. The estimated number of carriers generated at the highest fluence within a single NC was $\sim 10^7$

excitation. In these simulations we have assumed a Gaussian laser pulse envelop and a Beer's law dependence along the depth of the material. The ambipolar diffusion coefficient is represented by D in the above differential equation, τ is the relaxation time constant of the photo-generated carriers, and γ is the Auger coefficient. The above differential equation was solved numerically using the method of finite differences and the carrier density values obtained were fitted to the experimental data of the induced absorption. Some of the important parameters used in the above simulations were the absorption coefficient at the pump excitation wavelength $\alpha = 8\times10^4$ cm^{-1} [30], and the ambipolar diffusion coefficient $D = 0.6$ cm^2 s^{-1} [31]. The Auger coefficient γ and the carrier relaxation τ were considered as fitting parameters. Here we should point out that a very accurate measurement of the absorbed fluence was necessary in these experiments since fitting parameters such as the Auger coefficient is strongly dependent on the actual photo-generated carrier density. Utilizing the photo-generated carrier densities obtained under different fluence conditions it was possible to determine best-fitting results for each of the fluences (Fig. 4). The precise value of the Auger coefficient was mainly determined from the recovery shape of the induced absorption in the first tens of picoseconds, where the longer decay behavior determined the relaxation time constant τ for the carriers. Utilizing the above best-fit results for each of the photo-generated carrier density, it was possible to obtain an average value for the Auger coefficient $\gamma = 5.9 \pm 0.4 \times 10^{-31}$ cm^6 s^{-1} and carrier relaxation time constant $\tau = 110 \pm 10$ ps. We should note that the value of the Auger coefficient is similar to the value of bulk silicon [32]

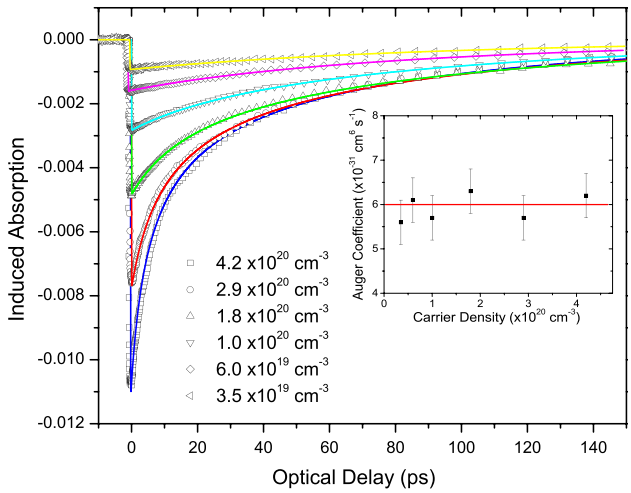

Fig. 4 Fitting results (represented by *straight lines*) of the experimental differential absorption (represented by *symbols*) of In_2O_3 NCs excited with 325 nm and probe at 350 nm. The fitting results were obtained from the simple differential equation model describing the carrier dynamics following ultrafast pulse excitation. The inset shows the Auger coefficient value for each of the fitted carrier density-induced absorption data (fluence)

which is 3.8×10^{-31} cm^6 s^{-1}. Furthermore, we should point out that given the large size of the NCs used in this study in comparison to the exciton Bohr radius no confinement [33, 34] or surface state effects [35] may play a significant role in the Auger dynamics.

In conclusion we have investigated ultrafast carrier dynamics in In_2O_3 NCs using pump-probe differential absorption white light measurements. State filling has been observed for probing wavelengths corresponding to energies above the band gap (3.5 eV) and just below the band edge due existence of shallow trap states. Positive-induced absorption (free carrier absorption) was the main contribution for wavelengths longer than 500 nm. Auger recombination appears to play a crucial role in the recovery of the photo-generated carriers in the first tens of ps. A simple differential equation model incorporating diffusion as well as carrier relaxation terms has provided a means to fit fluence dependence experimental data and obtain best-fit values for Auger recombination. The average Auger coefficient obtained from the fitted results was $\gamma = 5.9 \pm 0.4 \times 10^{-31}$ cm^6 s^{-1} and carrier relaxation time constant $\tau = 110 \pm 10$ ps. Finally, differential absorption data clearly shows a long delay (approximately 25 ps) for the carriers to reach the probing states, which are believed to be deep traps states and $\sim$300 ps for these carriers to move out of these states.

Acknowledgments The study in this article was partially supported by the research programs: EPYNE/0504/06, ERYAN/0506/04, and ERYNE/0506/02 funded by the Cyprus Research Promotion Foundation in Cyprus.

References

1. C. Li, D. Zhang, S. Han, X. Liu, T. Tang, B. Lei, Z. Liu, C. Zhou, Ann. N.Y. Acad. Sci. **1006**, 104 (2003). doi:10.1196/annals.1292.007
2. D.S. Ginley, C. Bright, Mater. Res. Soc. Bull. **25**, 15 (2000)
3. A. Gurlo, N. Barsan, U. Weimar, M. Ivanovskaya, A. Taurino, P. Siciliano, Chem. Mater. **15**, 4377 (2003). doi:10.1021/cm031114n
4. M.J. Zheng, L.D. Zhang, X.Y. Zhang, J. Zhang, G.H. Li, Chem. Phys. Lett. **334**, 298 (2001). doi:10.1016/S0009-2614(00)01426-3
5. C. Li, D.H. Zhang, S. Han, X.L. Liu, T. Tang, C.W. Zhou, Adv. Mater. **15**, 143 (2003). doi:10.1002/adma.200390029
6. L. Dai, X.L. Chen, J.K. Jian, M. He, T. Zhou, B.Q. Hu, Appl. Phys. A **75**, 687 (2002). doi:10.1007/s00339-002-1475-8
7. G.F. Zheng, F. Patolsky, Y. Cui, W.U. Wang, C.M. Lieber, Nat. Biotechnol. **23**, 1294 (2005). doi:10.1038/nbt1138
8. A. Kolmakov, D.O. Klenov, Y. Lilach, S. Stemmer, M. Moskovits, Nano. Lett. **5**, 667 (2005). doi:10.1021/nl050082v
9. Y. Cui, Q.Q. Wei, H.K. Park, C.M. Lieber, Science **293**, 1289 (2001). doi:10.1126/science.1062711
10. Z.H. Zhong, D.L. Wang, Y. Cui, M.W. Bockrath, C.M. Lieber, Science **302**, 1377 (2003). doi:10.1126/science.1090899
11. J. Zhang, X. Qing, F.H. Jiang, Z.H. Dai, Chem. Phys. Lett. **371**, 311 (2003). doi:10.1016/S0009-2614(03)00272-0
12. X.Y. Kong, Z.L. Wang, Solid State Commun. **128**, 1 (2003). doi:10.1016/S0038-1098(03)00650-1
13. H.J. Chun, Y.S. Choi, S.Y. Bae, H.C. Choi, J. Park, Appl. Phys. Lett. **85**, 461 (2004). doi:10.1063/1.1771816
14. P. Nguyen, H.T. Ng, T. Yamada, M.K. Smith, J. Li, J. Han, M. Meyyappan, Nano. Lett. **4**, 651 (2004). doi:10.1021/nl0498536
15. S.Y. Li, C.Y. Lee, P. Lin, T.Y. Tseng, Nanotechnology **16**, 451 (2005). doi:10.1088/0957-4484/16/4/021
16. T. Tang, X. Liu, C. Li, B. Lei, D. Zhang, M. Rouhanizadeh, T. Hsiai, C. Zhou, Appl. Phys. Lett. **86**, 103–903 (2005)
17. C. Li, B. Lei, D. Zhang, X. Liu, S. Han, T. Tang, M. Rouhanizadeh, T. Hsiai, C. Zhou, Appl. Phys. Lett. **83**, 4014 (2003). doi:10.1063/1.1625421
18. D. Zhang, Z. Liu, C. Li, T. Tang, X. Liu, S. Han, B. Lei, C. Zhou, Nano. Lett. **4**, 1919 (2004). doi:10.1021/nl0489283
19. D. Zhang, C. Li, S. Han, X. Liu, T. Tang, W. Jin, C. Zhou, Appl. Phys. A **77**, 163 (2003). doi:10.1007/s00339-003-2099-3
20. A. Othonos, J. Appl. Phys. **83**, 1789 (1998). doi:10.1063/1.367411
21. A. Othonos, E. Lioudakis, U. Philipose, H.E. Ruda, Appl. Phys. Lett. **91**, 241113 (2007). doi:10.1063/1.2825290
22. A. Othonos, M. Zervos, M. Pervolaraki, Nanoscale Res. Lett. **4**, 122 (2009). doi:10.1007/s11671-008-9211-8
23. M. Zervos, D. Tsokkou, M. Pervolaraki, A. Othonos, Nanoscale Res. Lett. (2009). doi:10.1007/s11671-009-9266-1
24. Z.M. Jarzebski, Phys. Status Solidi. A **71**, 13 (1982). doi:10.1002/pssa.2210710102
25. F. Zeng, X. Zhang, J. Wang, L. Zhang, Nanotechnology **15**, 596 (2004). doi:10.1088/0957-4484/15/5/033
26. S. Kar, S. Chaudhuri, Chem. Phys. Lett. **422**, 424 (2006). doi:10.1016/j.cplett.2006.03.002
27. M. Mazzera, M. Zha, D. Calestani, A. Zapettini, L. Lazzarini, G. Salviati, L. Zanotti, Nanotechnology **18**, 355707 (2007). doi:10.1088/0957-4484/18/35/355707
28. D. Calestani, M. Zha, A. Zapettini, L. Lazzarini, L. Zanotti, Chem. Phys. Lett. **445**, 251 (2007). doi:10.1016/j.cplett.2007.07.089
29. M. Kumar, V.N. Singh, F. Singh, K.V. Lakshm, B.R. Mehta, J.P. Singh, Appl. Phys. Lett. **92**, 171907 (2008). doi:10.1063/1.2910501

30. I. Hamberg, C.G. Granqvist, J. Appl. Phys. **60**, R123 (1986). doi:10.1063/1.337534
31. K.R. Murali, V. Sambasivam, J. Mater. Sci. Lett. **9**, 454 (1990). doi:10.1007/BF00721028
32. J. Dwiezor, W. Schmid, Appl. Phys. Lett. **31**, 346 (1977). doi:10.1063/1.89694
33. V.I. Klimov, A.A. Mikhailovsky, D.W. McBranch, C.A. Leatherdale, M.G. Bawendi, Science **287**, 1011 (2000). doi:10.1126/science.287.5455.1011
34. A.L. Efros, V.A. Kharchenko, M. Rosen, Solid State Commun. **93**, 281 (1995). doi:10.1016/0038-1098(94)00780-2
35. A. Othonos, M. Lioudakis, A.G. Nassiopoulou, Nanoscale Res. Lett. **3**, 315 (2008). doi:10.1007/s11671-008-9159-8